Dalton Transactions

ROYAL SOCIETY OF CHEMISTRY

PAPER

View Article Online
View Journal | View Issue

Check for updates

Cite this: *Dalton Trans.*, 2025, **54**, 2793

Anionic modulation induces molecular polarity in a three-component crown ether system†

Feiyan Liu, Guoyong Chen, Xiao Liu, Ting Jiang, Wenjing Guo,* Xiancai Li* and Zhenhong Wei *

Received 16th December 2024,
Accepted 3rd January 2025

DOI: 10.1039/d4dt03466j

rsc.li/dalton

Three-component crown ether phase change materials are characterized by a structural phase change in response to external stimuli such as temperature and electric or magnetic fields, resulting in significant changes in physical properties. In this work, we designed and synthesized two novel host–guest crown ether molecules [(PTFMA)(15-crown-5)ClO_4] (**1**) and [(PTFMA)(15-crown-5)PF_6] (**2**), through the reaction of *p*-trifluoromethylaniline (PTFMA) with 15-crown-5 in perchloric acid or hexafluorophosphoric acid aqueous solution. Compound **1** undergoes a structural change from the non-centrosymmetric space group ($P2_1$) to the centrosymmetric space group ($P2_1/c$) with increasing temperature. This transformation is accompanied by a switchable second harmonic generation (SHG) signal, a noticeable dielectric response, and a reversible phase transition in differential scanning calorimetry (DSC). For compound **2**, there are reversible phase transitions accompanied by a dielectric response, but it does not exhibit a switchable SHG signal. The difference in properties between the two compounds may be due to the polarity modulation of the anion, providing new ideas for obtaining crown ether complexes with SHG response properties.

Published on 06 January 2025. Downloaded on 5/1/2025 4:56:19 PM.

Introduction

Over the past decades, molecular rotors have played a key role in biomedicine, molecular sensing, controlled nonlinear optical switching materials, and piezoelectric materials, among many other areas, attracting a great deal of attention.[1–6] A molecular rotor usually consists of a stator and a rotor as well as a rotating shaft, with the stator always remaining relatively stationary while the rotor is in operation.[7–10] A three-component crown ether phase change material is a typical example of a molecular rotor material, where the crown ether acts as a stator, anchoring the organic amine *via* N–H···O hydrogen bonding, and the anion is used for charge balancing.[11–14] It has been shown that crown ether-based rotor–stator materials exhibit stable and excellent electro-optical and thermal properties, especially ferroelectric and dielectric properties, which have garnered considerable attention.[10]

The crown ether as a stator is a macrocyclic ether containing several oxygen atoms, which allows it to complex with positively charged ions, especially alkali metal ions.[15–17] Most importantly, crown ethers can also form complexes with amine ions through hydrogen bonding. Studies on crown ether host–guest compounds have primarily focused on 18-crown-6. To date, various phase change materials with favorable properties have been constructed using 18-crown-6 based host–guest compounds, including [($ClCH_2CH_2NH_3$)-(18-crown-6)][ClO_4],[1] [(MeO-C_6H_4-NH_3)(18-crown-6)][TFSA] (TFSA = bis(trifluoromethanesulfonyl)ammonium),[8] [(DIPA)(18-crown-6)] [BF_4] (DIPA = 2,6-diisopropylanilinium),[18] *etc*. However, there have been fewer reports focusing on 15-crown-5 in primary-guest compounds, and the available reports on the subject tend to focus on the phase transition and dielectric response, with little exploration of second harmonic (SHG) effects. This could be attributed to the fact that most host–guest crown ether complexes typically crystallize in centrosymmetric space groups, whereas the SHG effect requires the crystal structure to possess non-central symmetry.[19–24] Therefore, achieving crown ether complexes with SHG-responsive properties through exquisite structural modulation has become a major challenge in the field.

In view of this situation, the special nonlinear optical properties of SHG materials and their unique application potential increasingly highlight the value of in-depth studies.[25–29] The secondary nonlinear optical material can be reversibly

School of Chemistry and Chemical Engineering, Nanchang University, Nanchang, 330031, People's Republic of China.
E-mail: 352800220014@email.ncu.edu.cn, xcli@ncu.edu.cn, weizh@ncu.edu.cn

† Electronic supplementary information (ESI) available: FT-IR, PXRD pattern and structural parameter tables. CCDC 2408525 (200 K), 2408526 (273 K) (**1**) and 2408527 (200 K) (**2**). For ESI and crystallographic data in CIF or other electronic format see DOI: https://doi.org/10.1039/d4dt03466j

Published on 06 January 2025. Downloaded on 5/1/2025 4:56:19 PM.

switched from SHG-ON to SHG-OFF under appropriate external stimuli such as light, heat, or electricity.[30] In particular, the crown ether subject–guest compounds move from one equilibrium state to another under the stimulus of external temperature, and this process favors the induction of the SHG effect.[31–33]

Fu *et al.* designed host–guest type phase transition supramolecular inclusions, $[(ClCH_2CH_2NH_3)(18\text{-crown-6})][ClO_4]$ and $[(ClCH_2CH_2NH_3)\text{-}(18\text{-crown-6})][PF_6]$, which exhibited high phase transition temperatures of 363 K and 343 K, respectively.[1] The observed internal anionic differences lead to a difference in their phase transition temperatures of 20 K, which illustrates the principle of regulating the phase transition point through the use of inorganic anions. Based on this idea, we aim to develop novel phase change materials and crown ether complexes with multi-switching response properties. To achieve this, we selected perchloric acid and hexafluorophosphoric acid as inorganic anions and screened *p*-trifluoromethylaniline as a promising organic cation.

As a result, we designed and synthesized two new crown ether host–guest compounds: $[(PTFMA)(15\text{-crown-5})ClO_4]$ (**1**) and $[(PTFMA)\text{-}(15\text{-crown-5})PF_6]$ (**2**) (Scheme 1). Both compounds exhibit a pair of reversible phase transitions at 244 K/231 K and 316 K/305 K, respectively, accompanied by a significant dielectric response during the phase transitions. Notably, compound **1** also demonstrates a switchable SHG signal. The distinct properties observed between the two compounds are predominantly ascribed to the regulation of anion polarity. This study not only reinforces the concept of utilizing anionic variations to influence phase transition behavior but also provides new insights into the discovery of innovative phase transition materials and crown ether complexes with multi-switching response properties.

Experimental

Materials

p-Trifluoromethylaniline, 15-crown-5, and hexafluorophosphoric acid (70%) are purchased from Damas-Beta. All reagents do not require further purification.

Synthesis

$[(PTFMA)(15\text{-crown-5})ClO_4]$ (1). A solution containing 0.16 g (1 mmol) of *p*-trifluoromethylaniline in 10 mL of methanol is prepared, to which 90 μL of 70% $HClO_4$ is gradually added. The mixture is stirred for ten minutes, followed by the addition of 0.22 g (1 mmol) of 15-crown-5, after which stirring continues for thirty minutes. The resulting clear solution is allowed to evaporate at room temperature for three days, yielding white crystals. Yield: 0.22 g, 44.9%. Elemental analysis: calculated, C 42.33%, H 5.60%, N 2.90%; found, C 42.77%, H 5.26%, N 3.21%. IR (KBr disc, cm^{-1}): 3067(m), 2924(m), 2873(m), 1323(s), 1244(m), 1051(s), 935(s), 853(m), 827(m), 747(m).

$[(PTFMA)(15\text{-crown-5})PF_6]$ (2). Following a similar method to that used to synthesize compound **1**, 0.16 g (1 mmol) *p*-trifluoromethylaniline, 136 μL of 70% HPF_6, and 0.22 g (1 mmol) 15-crown-5 were combined to produce white crystals of compound **2**. Yield: 0.27 g, 51.0%. Elemental analysis: calculated, C 38.68%, H 5.12%, N 2.63%; found, C 39.12%, H 5.67%, N 2.96%. IR (KBr disc, cm^{-1}): 3242(m), 3035(m), 2905(m), 2870(m), 1321(s), 1248(m), 1048(s), 941(s), 820(s).

Results and discussion

Synthesis and characterization

White transparent crystals of compounds **1** and **2** are powdered for various characterization studies. The purity of compounds **1** and **2** is demonstrated by powder X-ray diffraction (Fig. S1†) and elemental analysis. Infrared spectroscopy revealed that distinct peaks of Cl–O, C–F, and C–N bonds in compound **1** are at 1051 cm^{-1}, 1323 cm^{-1}, and 1244 cm^{-1}, whereas the characteristic absorption peaks of C–F, C–N, and P–F bonds in compound **2** are at 1321 cm^{-1}, 1248 cm^{-1}, and 820 cm^{-1} (Fig. S2†). According to the thermogravimetric test results, both compound **1** and compound **2** exhibit good thermal stability. Specifically, compound **1** remained stable until 170 °C, while compound **2** did not decompose until 180 °C, as shown in Fig. S3.†

Phase transition

The thermal properties of compounds **1** and **2** are characterized by differential scanning calorimetry (DSC). For compound **1**, there is a pair of reversible endothermic and exothermic peaks at 244 K/231 K, with a thermal hysteresis of 13 K (Fig. 1a). The obvious thermal hysteresis suggests a first-order phase transition. Similarly, compound **2** displays a pair of switchable endothermic and exothermic peaks at 316 K/305 K, with a thermal hysteresis of 11 K, indicating that the phase

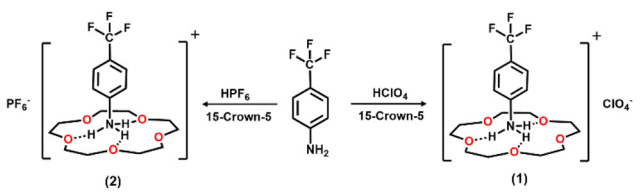

Scheme 1 Synthesis routes of compounds **1** and **2**.

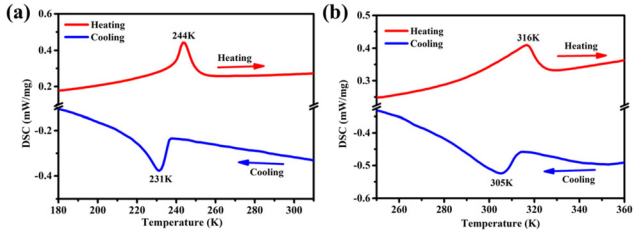

Fig. 1 DSC curves of **1** (a) and **2** (b) in heating and cooling runs.

This journal is © The Royal Society of Chemistry 2025

Published on 06 January 2025. Downloaded on 5/1/2025 4:56:19 PM.

change is also a first-order phase transition (Fig. 1b). It can be seen that the phase transition temperature of compound **2** is 71 K higher than that of compound **1**, and we speculate that it is due to the stronger ionic interactions of hexafluorophosphate compared to perchlorate. This stronger interaction leads to closer intermolecular bonding in the products, contributing to the higher phase transition temperature.

As shown in Table 1, the value of ΔH for compound **1** at a phase transition temperature of 244 K is obtained instrumentally, and the ΔS is calculated to be 7.17 J mol^{-1} K^{-1}. According to the Boltzmann equation $\Delta S = R \ln N$ (where R = 8.314 is the gas constant and N represents the geometrically based ratio of the orientation numbers),[34] the value of N is obtained as 2.37. The ΔS value for compound **2** is calculated in the same way to be 3.29 J mol^{-1} K^{-1} with an N value of 1.49. The calorimetric analysis of the phase transitions for both compounds reveals that their structural phase transitions are categorized as ordered–disordered transitions.

Dielectric properties

Dielectric anomalies often arise near phase transitions, making dielectric response a useful tool for confirming these transitions.[35,36] The dielectrics of compounds **1** and **2** are measured at different temperatures, and the results are shown in Fig. 2. Compounds **1** and **2** show significant dielectric anomalies at around 244 K and 316 K, respectively (Fig. 2a and b). Specifically, compounds **1** and **2** show dielectric changes near the phase transition of about 1.5 times and 2 times, respectively, with dielectric constants as high as 27 and 30 Fm^{-1}. This is mainly due to the change of the acid radical ions (anions) from ordered to disordered with increasing temperature. This change in anion configuration leads to a shift of the dielectric anomaly of compound **2** towards higher temperatures and a significant enhancement of the dielectric strength as well, suggesting that modifying the anion can effectively modulate the dielectric properties of the compounds. As shown in Fig. 2c and d, the trend of dielectric anomalies during the cooling process of compounds **1** and **2** at 1 MHz is consistent with the heating phase and also corresponds to the reversible phase transition occurring in DSC.

Table 1 The thermal values in the phase transitions of **1–2**

Compounds	PT (K)	ΔH (KJ mol^{-1})	ΔS (J mol^{-1} K^{-1})	N
1	344	1.75	7.17	2.37
2	316	1.04	3.29	1.49

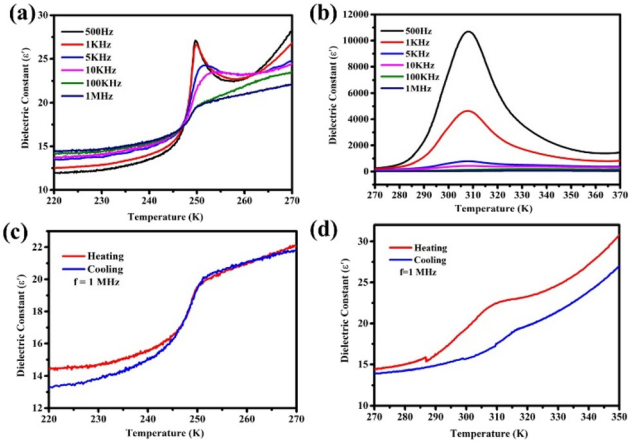

Fig. 2 Temperature-dependent real part (ε') of the dielectric constant at different frequencies measured for **1** (a) and **2** (b). Variation of ε' of **1** (c) and **2** (d) with temperatures at 1 MHz.

Variable temperature crystal structure analysis

To gain a deeper understanding of the causes of phase transitions and dielectric generation, we tested the crystal structures of compounds **1** and **2** at different temperatures. Compound **1** crystallized in the monoclinic $P2_1$ space group (point group C_2) under the low temperature phase (LTP) at 200 K. The asymmetric unit contains two three-component molecules [(PTFMA)(15-crown-5) ClO_4] (with half of the unit structure shown in Fig. 3a). The lattice parameters are as follows: a = 14.5944(5) Å, b = 9.4697(2) Å, c = 17.1687(5) Å, $\alpha = \gamma$ = 90°, and β = 111.882(4)° (Table S1†). As shown in Fig. 3a, the hydrogen atoms attached to the nitrogen atoms interact with the oxygen atoms in the crown ether and perchloric acid, forming two distinct types of N–H···O hydrogen bonds (for details see Table S2†). However, hydrogen bonding exists only between *p*-trifluoromethylaniline, 15-crown-5 and perchloric acid within a single molecule, resulting in the formation of a zero-dimensional single-crystal structure (Fig. S4†).

At 293 K, which corresponds to the high-temperature phase transition (HTP), the space group of compound **1** changes to the monoclinic $P2_1/c$ space group (point group C_{2h}). The lattice parameters are modified as follows: a = 14.9120(11) Å, b = 9.6790(5) Å, c = 16.9652(12) Å, α = 90°, β = 111.895(9) °, and γ = 90°. The symmetry of the crystal decreases as the temperature changes from the $P2_1$ to the $P2_1/c$ space group before and after the phase transition. The asymmetric unit comprises one three-component molecule [(PTFMA)(15-crown-5)ClO_4], as shown in Fig. 3c. In the HTP, the Cl–O bond length varies from 1.307 Å to 1.467 Å and the O–Cl–O bond angle ranges from 102.9° to 115.1°, and the average Cl–O bond length and the average O–Cl–O bond angle are comparatively larger in the HTP than in the LTP (Table S3†). At the same time, the N–H···O hydrogen bond length between the $(PTFMA)^+$ cation and the anion (ClO_4^-) becomes longer, indicating a weaker interaction between the cation and anion. This may be due to a change in perchloric acid from ordered to disordered as the temperature increases.

In order to more visually compare the structural differences between compounds **1** and **2**, a variable temperature single crystal structure analysis is conducted on compound **2**. Unfortunately, data are only obtained at 200 K. At 200 K (LTP), compound **2** crystallizes in the monoclinic crystal system within the $P2_1/n$ space group. The lattice parameters are as follows: a = 10.5818(4) Å, b = 15.9181(6) Å, c = 13.8015(5), α =

Published on 06 January 2025. Downloaded on 5/1/2025 4:56:19 PM.

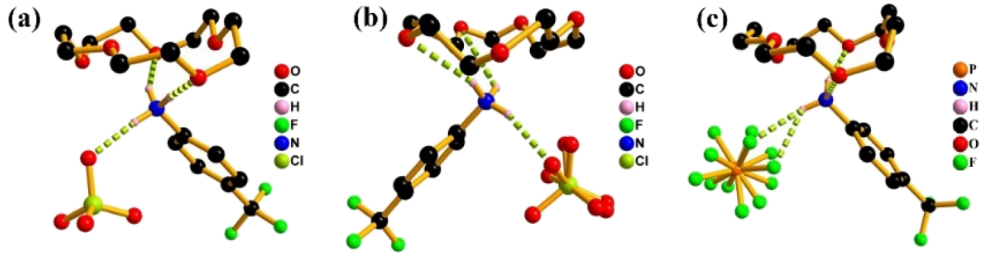

Fig. 3 Crystal structures of compounds **1** (a) and **2** (c) at 200 K, and crystal structures of compounds **1** (b) at 293 K.

90°, β = 93.642(3) °, and γ = 90° (Table S4†). An asymmetric unit comprises one three-component molecule, $[(C_7H_7F_3N)^+(15\text{-crown-}5)PF_6^-]$ (Fig. 3b). The hydrogen atoms on N form strong N–H···O hydrogen bonds with the oxygen in the crown ether, and N–H···F hydrogen bonds with the fluorine atoms in PF_6^- (Table S5†). The bond lengths of F–P range from 1.475(9) Å to 1.714(6) Å, and the bond angles of F–P–F range from 80.9°(5) to 169.0°(3) (Table S6†), indicating that PF_6^- is not an *ortho*-octahedron. This may be influenced by the fact that the hydrogen atoms attached to the nitrogen atoms also form an N–H···F hydrogen bond with the fluorine atom in the hexafluorophosphate root.

Since compound **2** exhibits significant disorder at high temperatures, it is not possible to obtain single-crystal data for its high-temperature phase. To further understand the structural changes of the compounds, we test variable temperature X-ray powder diffraction of compound **2** (Fig. 4). Below 316 K (prior to the phase transition), the XRD spectral lines remain nearly unchanged. However, the number of diffraction peaks at 10.4°–11.9°, 15°–15.5°, 20.1°–22.0°, and 23.5°–24.2° is significantly reduced when the phase transition point is exceeded. The obvious changes in the variable temperature XRD results indicate the occurrence of a phase transition, which is consistent with the DSC results.

SHG effect

The symmetry of crystals plays an important role in the physical properties of compounds. Among these properties, the switching of the SHG signal is closely related to the symmetry of the crystal.[36–40] The signal of SHG can only correspond to non-centrosymmetric crystals (NCS).[41,42] Through testing, it is found that compound **1** exhibits a switchable SHG signal (Fig. 5a), while compound **2** displays almost no SHG signal. Before the phase transition, compound **1**, while in the $P2_1$ non-center space group, has an SHG signal with a signal value 0.15 times that of KDP (Fig. S5†). As the temperature rises, the SHG signal gradually weakens. When the temperature approximates 244 K, the SHG signal value approaches zero, and at this point, the space group changes to $P2_1/c$. The transition of the SHG signal from presence to absence corresponds to the change in the crystal's spatial symmetry from non-centrosymmetric to centrosymmetric, reflecting the pair of reversible phase transitions observed in DSC. During this process, the ClO_4^- anion of compound **1** undergoes a transition from order to disorder. This indicates that compound **1** has a switchable SHG signal that achieves the transition from SHG-ON to SHG-OFF. To verify the durability of this signal switching, a six-cycle test is performed. The results (Fig. 5b) indicate that the passing signal slightly decreases in the first three cycles but remains relatively stable in the subsequent cycles. This also indicates that the SHG signal switching of compound **1** is still relatively persistent. Combined with the above characterization studies, this suggests that compound **1** may be a potential ferroelectric material, as shown in Fig. S6.†

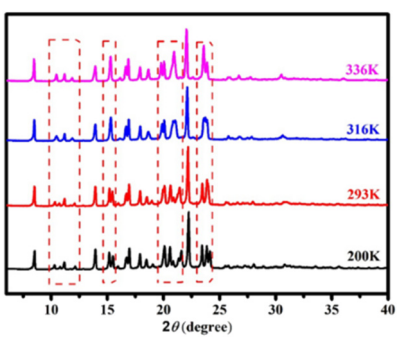

Fig. 4 Variable temperature XRD plot for compound **2**.

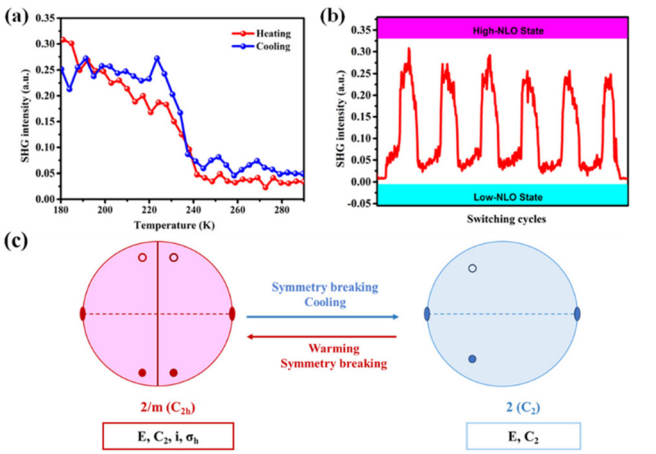

Fig. 5 (a) SHG signaling plot of compound **1**. (b) SHG cycle diagram of compound **1**. (c) Stark surface projections of compound **1** in the low-temperature phase ($P2_1$) and the high-temperature phase ($P2_1/c$).

This journal is © The Royal Society of Chemistry 2025

Published on 06 January 2025. Downloaded on 5/1/2025 4:56:19 PM.

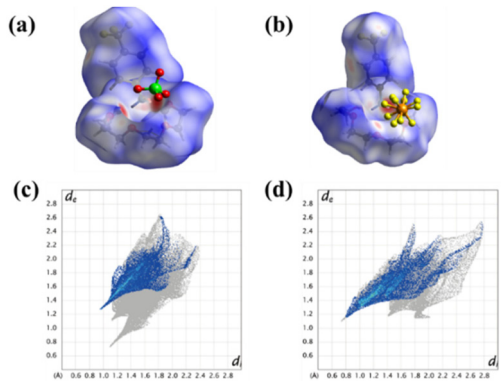

Fig. 6 The Hirshfeld dnorm surface plots of **1** (a) and **2** (b) and the fingerprints of **1** (c) and **2** (d).

In addition, SHG is a tool used to probe the importance of inversion center symmetry breaking during phase transitions.[43–46] For this purpose, we plot the terrestrial projection of compound **1** from the LTP to the HTP. In the LTP, compound **1** is in the $P2_1$ space group in point group **2**, which contains two symmetry elements: E and C_2. In the HTP, compound **1** is in the $P2_1/c$ space group in point group $2/m$, with four symmetry elements E, C_2, i, and σ_h. As the system transitions from the HTP to the LTP, symmetry breaking occurs, accompanied by the disappearance of two symmetry elements: i and σ_h. The changes in the symmetry elements and the changes in the micro-symmetry operation reflected in the space group changes are consistent with the switching of the SHG signal.

Hirshfeld dnorm surface and the fingerprint analysis

In order to study the interaction forces within molecules, Hirshfeld d_{norm} surfaces and two-dimensional (2D) fingerprint maps are created, as shown in Fig. 6. We consider the crown ether and the amine as a whole and explore the force of the anion on this entire system. The interaction of the oxygen atom in the anion (ClO_4^-) with its surroundings is calculated to be 19.2% in compound **1**. In contrast, the fluorine atom in the anion of compound **2** (PF_6^-) interacts with the surrounding environment to a degree of 28.8%. The anionic force on the crown ether and amine in compound **2** is greater than that in compound **1**. This also provides a plausible explanation for the greater phase transition temperature for compound **2** than for compound **1**.

Conclusions

In conclusion, two three-component crown ether phase change material molecules, [(PTFMA)(15-crown-5)ClO_4] (**1**) and [(PTFMA) (15-crown-5)PF_6] (**2**), are synthesized in this work. Compound **1** exhibits a pair of reversible phase transitions at 244 K/231 K, with a space group shift from $P2_1$ to $P2_1/c$, the presence of a switchable SHG signal, and an accompanying pronounced dielectric response. Compound **2** shows a pair of reversible DSC phase transitions at 316 K/305 K and always remains in the center space group. Structural analysis indicates that the difference in the properties of compounds **1** and **2** results from anionic polarity modulation. This also provides ideas for the discovery of new three-component crown ether phase change materials with switchable SHG signals.

Author contributions

L. F. Y. prepared the samples, measured the properties, and wrote the manuscript. C. G. Y., L. X. and J. T. determined the structures. G. W. J., L. X. C. and W. Z. H. provided suggestions for research.

Data availability

The data supporting this article have been included as part of the ESI.†

Conflicts of interest

There are no conflicts to declare.

Acknowledgements

This work was supported by the National Natural Science Foundation of China (22071094 and 22075123) and the Department of Science and Technology in Jiangxi Province (20213BCJ22055 and 20224ACB203004).

References

1 Y.-F. Gao, Z.-X. Zhang, T. Zhang, C.-Y. Su, W.-Y. Zhang and D.-W. Fu, *Mater. Chem. Front.*, 2020, **4**, 3003–3012.
2 N. Song, T.-T. Ying, Y.-H. Tan, Y.-Z. Tang, J. Liao, L.-J. Wang, F.-X. Wang and M.-Y. Wan, *Dalton Trans.*, 2023, **52**, 11196–11202.
3 N. Wang, H.-K. Li, H.-Y. Shen, L. Ye, Z.-J. Xu, M.-L. Ren, N.-T. Yao, C. Shi, H.-Y. Ye and L.-P. Miao, *Angew. Chem., Int. Ed.*, 2024, e202421298.
4 H.-Y. Ye, S.-H. Li, Y. Zhang, L. Zhou, F. Deng and R.-G. Xiong, *J. Am. Chem. Soc.*, 2014, **136**, 10033–10040.
5 X. Ye, W. He, J. Wei, Z. Wei, X. You and H. Cai, *Dalton Trans.*, 2022, **51**, 15074–15079.
6 F.-F. Di, L. Zhou, W.-J. Chen, J.-C. Liu, H. Peng, S.-Y. Tang, H. Yu, W.-Q. Liao and Z.-X. Wang, *Inorg. Chem. Front.*, 2021, **8**, 4896–4902.
7 Y.-F. Zhang, F.-F. Di, P.-F. Li and R.-G. Xiong, *Chem. – Eur. J.*, 2022, **28**, e202102990.
8 X.-J. Song, T. Zhang, Z.-X. Gu, Z.-X. Zhang, D.-W. Fu, X.-G. Chen, H.-Y. Zhang and R.-G. Xiong, *J. Am. Chem. Soc.*, 2021, **143**, 5091–5098.

Published on 06 January 2025. Downloaded on 5/1/2025 4:56:19 PM.

9 S. Mandal, T. K. Mukhopadhyay and A. Datta, *J. Phys. Chem. C*, 2023, **127**, 18206–18212.
10 Y.-L. Wei, J. Jing, C. Shi, H.-Y. Ye, Z.-X. Wang and Y. Zhang, *Chem. Commun.*, 2018, **54**, 8076–8079.
11 H.-P. Lv, Y.-R. Li, X.-J. Song, N. Zhang, R.-G. Xiong and H.-Y. Zhang, *J. Am. Chem. Soc.*, 2023, **145**, 3187–3195.
12 M.-M. Lun, C.-Y. Su, Q.-Q. Jia, Z.-X. Zhang, J. Li, H.-F. Lu, Y. Zhang and D.-W. Fu, *Inorg. Chem. Front.*, 2023, **10**, 5026–5034.
13 W. Li, C.-T. He, Y. Zeng, C.-M. Ji, Z.-Y. Du, W.-X. Zhang and X.-M. Chen, *J. Am. Chem. Soc.*, 2017, **139**, 8086–8089.
14 H.-Y. Zhang, S.-Q. Lu, X. Chen, R.-G. Xiong and Y.-Y. Tang, *Chem. Commun.*, 2019, **55**, 11571–11574.
15 Y.-R. Li, Y.-F. Zhang, Y.-Y. Tang and H.-Y. Zhang, *Chem. Commun.*, 2022, **58**, 5148–5151.
16 J.-C. Liu, F.-F. Di, Y.-P. Zeng, W.-J. Chen, X.-Y. Huang, Y.-L. Luo, X. Zhu, L. Zhou and Y.-Y. Tang, *Inorg. Chem. Front.*, 2022, **9**, 5799–5804.
17 M.-M. Lun, T. Zhang, C.-Y. Su, J. Li, Z.-X. Zhang, D.-W. Fu and H.-F. Lu, *Mater. Chem. Front.*, 2022, **6**, 1929–1937.
18 Y. Zhang, H.-Y. Ye, D.-W. Fu and R.-G. Xiong, *Angew. Chem., Int. Ed.*, 2014, **53**, 2114–2118.
19 Z. Yu, T. Wang, G. Wang, K. Xu, Q. Cui, L. Cao and B. Teng, *CrystEngComm*, 2020, **22**, 8362–8373.
20 Q. Zhu, K. Zhang, D. Li, N. Li, J. Xu, D. W. Bahnemann and C. Wang, *Chem. Eng. J.*, 2021, **426**, 131681.
21 Q. Ding, X. Liu, S. Zhao, Y. Wang, Y. Li, L. Li, S. Liu, Z. Lin, M. Hong and J. Luo, *J. Am. Chem. Soc.*, 2020, **142**, 6472–6476.
22 D. C. Han, Y. H. Tan, Y. K. Li, J. H. Wen, Y. Z. Tang, W. J. Wei, P. K. Du and H. Zhang, *Chem. – Eur. J.*, 2021, **27**, 13575–13581.31.
23 H. Zhang, X. You, M. Zhang, W. Guo, Z. Wei and H. Cai, *Dalton Trans.*, 2023, **52**, 1753–1760.
24 F. Jiang, C.-F. Wang, Y.-X. Wu, H.-H. Li, C. Shi, H.-Y. Ye and Y. Zhang, *J. Phys. Chem. C*, 2020, **124**, 5796–5801.
25 Y.-Z. Zhang, D.-S. Sun, J.-X. Gao, X.-N. Hua, X.-G. Chen, G.-Q. Mei and W.-Q. Liao, *Chem. – Asian J.*, 2019, **14**, 1028–1033.
26 S.-L. Li, H.-M. Xu, Y. Zhang, W. Yang, Z. Qi, J. Zhang and X.-M. Zhang, *Cryst. Growth Des.*, 2021, **21**, 5752–5759.
27 S. A. Denev, T. T. A. Lummen, E. Barnes, A. Kumar and V. Gopalan, *J. Am. Ceram. Soc.*, 2011, **94**, 2699–2727.
28 J. Jing, F. Jiang, Y.-L. Wei, C. Shi, H.-Y. Ye and Y. Zhang, *Crystals*, 2019, **9**, 184–191.
29 H.-Y. Zhang, Z.-X. Zhang, X.-G. Chen, X.-J. Song, Y. Zhang and R.-G. Xiong, *J. Am. Chem. Soc.*, 2021, **143**, 1664–1672.
30 H. Peng, Y.-H. Liu, X.-Q. Huang, Q. Liu, Z.-H. Yu, Z.-X. Wang and W.-Q. Liao, *Mater. Chem. Front.*, 2021, **5**, 4756–4763.
31 X.-R. Fan, M.-M. Lun, Z.-J. Wang, B.-W. Deng, D.-W. Fu, C.-F. Wang, H.-F. Lu and Z.-X. Zhang, *J. Mater. Chem. C*, 2023, **11**, 10051–10057.
32 H.-K. Li, W. Luo, L. Ye, Z.-J. Xu, M.-L. Ren, C. Shi, H.-Y. Ye, L.-P. Miao and N. Wang, *Cryst. Growth Des.*, 2024, **24**, 5411–5416.
33 Y. Liu, H.-T. Zhou, S.-P. Chen, Y.-H. Tan, C.-F. Wang, C.-S. Yang, H.-R. Wen and Y.-Z. Tang, *Dalton Trans.*, 2018, **47**, 3851–3856.
34 P.-F. Li, W.-Q. Liao, Y.-Y. Tang, W. Qiao, D. Zhao, Y. Ai, Y.-F. Yao and R.-G. Xiong, *Proc. Natl. Acad. Sci. U. S. A.*, 2019, **116**, 5878–5885.
35 Y. Zeng, J. Liu, L. Zhou, X. Deng, W. Yang, X. Yan, Y. Luo, X. Zhu, X. Huang, X. Song and Y. Tang, *Chin. Chem. Lett.*, 2023, **34**, 108127.
36 W. Guo, Z. Yang, L. Shu, H. Cai and Z. Wei, *Angew. Chem., Int. Ed.*, 2024, **63**, e202407934.
37 G.-Q. Mei, H.-Y. Zhang and W.-Q. Liao, *Chem. Commun.*, 2016, **52**, 11135–11138.
38 J. ZhenTao, H. Yanhuan, W. Hui, Z. Xiuxiu, Y. Jiaojiao, L. Mingli and W. Zhenhong, *J. Solid State Chem.*, 2020, **282**, 121104.
39 Y.-K. Li, T.-T. Ying, H. Zhang, Y.-H. Tan, Y.-Z. Tang, F.-X. Wang and M.-Y. Wan, *Dalton Trans.*, 2022, **51**, 6860–6867.
40 Y. Li, Y. Du, C.-R. Huang, H. Peng, Y.-L. Zeng, J.-C. Liu and W.-Q. Liao, *Chem. Commun.*, 2021, **57**, 5171–5174.
41 R. Chakraborty, P. K. Rajput, G. M. Anilkumar, S. Maqbool, R. Das, A. Rahman, P. Mandal and A. Nag, *J. Am. Chem. Soc.*, 2023, **145**, 1378–1388.
42 B. Wang, D. Ma, H. Zhao, L. Long and L. Zheng, *Inorg. Chem.*, 2019, **58**, 13953–13959.
43 W.-Y. Zhang, Y.-Y. Tang, P.-F. Li, P.-P. Shi, W.-Q. Liao, D.-W. Fu, H.-Y. Ye, Y. Zhang and R.-G. Xiong, *J. Am. Chem. Soc.*, 2017, **139**, 10897–10902.
44 W.-Q. Liao, Y.-Y. Tang, P.-F. Li, Y.-M. You and R.-G. Xiong, *J. Am. Chem. Soc.*, 2017, **139**, 18071–18077.
45 X. Liu, Z. Xu, P. Long, Y. Yao, C. Ji, L. Li, Z. Sun, M. Hong and J. Luo, *Chem. Mater.*, 2020, **32**, 8965–8970.
46 P.-P. Shi, Y.-Y. Tang, P.-F. Li, W.-Q. Liao, Z.-X. Wang, Q. Ye and R.-G. Xiong, *Chem. Soc. Rev.*, 2016, **45**, 3811–3827.

This journal is © The Royal Society of Chemistry 2025